



# Structure and electrochemical properties of magnetite and polypyrrole nanocomposites formed by pyrrole oxidation with magnetite nanoparticles

Monika Wysocka-Żołopa<sup>1</sup> · Aleksandra Brzózka<sup>1</sup> · Elżbieta Zambrzycka-Szelewa<sup>1</sup> · Urszula Klekotka<sup>1</sup> · Beata Kalska-Szostko<sup>1</sup> · Krzysztof Winkler<sup>1</sup>

Received: 13 February 2023 / Revised: 25 May 2023 / Accepted: 25 May 2023 / Published online: 21 June 2023  
© The Author(s) 2023

## Abstract

Nanocomposite of magnetic Fe<sub>3</sub>O<sub>4</sub> nanoparticles and polypyrrole was prepared under sonication by a new chemical polymerization method during which Fe<sub>3</sub>O<sub>4</sub> nanoparticles acted both as a pyrrole oxidant and as a component in the composite material. Synthesis of this nanocomposite was carried out in aqueous solution acidified to pH 2, a prerequisite for the formation of these types of material and to facilitate pyrrole oxidation by Fe<sub>3</sub>O<sub>4</sub> nanoparticles. In this way, two kind of materials were produced: Fe<sub>3</sub>O<sub>4</sub>/PPy nanocomposite in which magnetite nanoparticles were dispersed in PPy matrix and Fe<sub>3</sub>O<sub>4</sub>-aggregates@PPy nanocomposite that exhibits structure in which aggregates of magnetite nanoparticles are surrounded by a layer of polymeric phase. In the latter case, the polymerization process took place in the presence of a surfactant. These nanocomposites were characterized by electron microscopy techniques, IR spectroscopy, X-ray powder diffraction, X-ray photoelectron spectroscopy and thermogravimetry. Particular attention was focused on the study of the electrochemical properties of the formed composites. The composite of Fe<sub>3</sub>O<sub>4</sub> and PPy exhibits reversible electrochemical behaviour upon oxidation. The electrode process of the polymeric component oxidation in organic solvents such as acetonitrile and dichloromethane is very similar to the process in an aqueous solution.

**Keywords** Nanocomposites electrochemistry · Magnetic polymers · Polypyrroles · Core-shell nanoparticles

## Introduction

Conducting polymers have been intensively studied due to their due to their unique physicochemical properties. They exhibit good conductivity, convenient preparation methods, low production costs, good environmental stability and wide range of applications, especially in light-emitting, electronic devices, energy storage systems, (bio)sensors and solar cells [1–4]. Among the various conducting polymers, polypyrrole (PPy) has received particular attention because of its electrical conductivity, good redox properties and low production costs [5–7]. PPy-based materials show high electrical

conductivity and good redox reversibility. Additionally, they possess good thermal stability. Polypyrrole can also be used as a component of composite materials with carbon nanostructures. PPy can be prepared quite easily by either chemical or electrochemical polymerization of pyrrole [8–11]. Chemical polymerization of pyrrole occurs in the presence of various oxidizing agents such as iron(III) chloride, iron(III) sulfonates, iron(III) complexes, ammonium persulphate (APS), potassium dichromate (PDC) and H<sub>2</sub>O<sub>2</sub>. Polymerization under electrochemical conditions proceeds as a result of direct pyrrole electro-oxidation [9, 10] or is induced by an electrochemical process involving a redox couple, as in the case of the [Fe(CN)<sub>6</sub>]<sup>4-</sup>/[Fe(CN)<sub>6</sub>]<sup>3-</sup> [12]. The latter method was used to modify yeast cell walls with thin polypyrrole films [12, 13].

It is well known that the conductivity and morphology of polypyrrole depend significantly on the nature of the oxidant and the type of dopant used in the polymerization solutions. For example, Shinde et al. [14] obtained three different morphologies of polypyrrole particles, namely

✉ Monika Wysocka-Żołopa  
monia@uwb.edu.pl

✉ Krzysztof Winkler  
winkler@uwb.edu.pl

<sup>1</sup> Department of Chemistry, University of Białystok, Ciołkowskiego 1K, 15-245, Białystok, Poland

mud-like, cauliflower and interconnected structures during pyrrole polymerization using APS,  $\text{FeCl}_3$  and PDC as oxidant, respectively. From among these three morphologies, the material composed of interconnected polypyrrole nanoparticles was the only one to provide a unique three-dimensional network, large surface area and meso-porous structure required for better supercapacitive electrode materials. Goel et al. [15] prepared polypyrrole nanofibers using an interfacial oxidative polymerization procedure. Monomer was dissolved in chloroform phase and aqueous solution containing APS as an oxidation agent and different dopants including HCl,  $\text{FeCl}_3$ , *p*-toluene sulfonic acid (*p*-TSA), camphor sulfonic acid (CSA) and polystyrene sulfonic acid (PSSA). Conductivity of formed materials depends on the dopant. Conductivity ranging from  $2 \times 10^{-5} \text{ S cm}^{-1}$  to  $6 \times 10^{-2} \text{ S cm}^{-1}$  were observed for polypyrrole doped with PSSA and *p*-TSA, respectively. These changes in the conductive properties of the polymer are the result of the size of the dopants, their density in the polymer material and morphological changes accompanying the doping process. Better spatial arrangement of the dopant ions in the polypyrrole matrix usually leads to an improvement in the conductive properties of the material. A large enhancement of conductivity and significant modification of the polymeric phase morphology was also reported for polypyrrole synthesized in the presence of anionic surfactants [16]. A relatively strong ionic interaction between dopant and oxidized polypyrrole matrix results in the increase in the polymeric phase stability and better conducting properties.

Recently, magnetic nanomaterials also attracted much attention. Magnetic properties allow the potential use of these materials in colour imaging technology, ferrofluids, magnetic recording media and medical diagnostics [17–20]. Magnetite ( $\text{Fe}_3\text{O}_4$ ) is a representative example of such materials and is widely used due to its strong magnetic properties, large surface area and low toxicity which makes it suitable for various applications in biotechnology and medicine [21–23]. However, pure  $\text{Fe}_3\text{O}_4$  particles are very sensitive to oxidation due to their high chemical reactivity. They also exhibit tendency to form agglomerations in order to minimize their surface energy. These factors have limited their use to some extent. One of the main approaches to overcome these limitations is to protect pure magnetic particles with polymers [24–28] or inorganic shells such as metals [29, 30] or oxides [31]. The magnetite particles are usually formed through co-precipitation of Fe(II) and Fe(III) salts in an alkaline solution [32, 33]. Smaller and more uniform particles can be synthesized by using the microemulsion approach [34].

Numerous studies have investigated magnetic particles coated with conducting polymers, particularly  $\text{Fe}_3\text{O}_4$ /PPy composite nanostructures. For instance, Deng et al. [35] reported the preparation of  $\text{Fe}_3\text{O}_4$ /PPy nanoparticles with

a core-shell structure via a two-step process: synthesis of  $\text{Fe}_3\text{O}_4$  magnetic nanoparticles via the precipitation-oxidation method followed by in situ emulsion polymerization in aqueous solution containing sodium dodecylbenzenesulfonate as surfactant and dopant. Zhao and Nan [36] prepared stable magnetic nanofluids containing  $\text{Fe}_3\text{O}_4$ @PPy composites and studied their dispersion stability. Qiao et al. [37] also prepared  $\text{Fe}_3\text{O}_4$ @PPy composites by chemical oxidative polymerization in the presence of *poly*(vinyl alcohol) and *p*-toluenesulfonic acid (*p*-TSA). They obtained a polypyrrole shell thickness ranging from 20 to 80 nm due to the variability in the pyrrole/ $\text{Fe}_3\text{O}_4$  mass ratio. PPy/ $\text{Fe}_3\text{O}_4$  composite nanotubes with diameters of 250–400 nm and lengths of 20–50  $\mu\text{m}$  exhibiting both electrochemical and magnetic activity were synthesized by a self-assembly process using  $\text{FeCl}_3$  as oxidant and *p*-TSA as dopant [38].

In this study, we propose a new approach for the chemical synthesis of a composite composed of polypyrrole and  $\text{Fe}_3\text{O}_4$  nanoparticles, during which the  $\text{Fe}_3\text{O}_4$  nanoparticles act as both a pyrrole oxidant in the polymerization process and as a component in the composite material. In this case, the polymerization process is initiated at the nanoparticle surface to form a polymeric phase. The morphology of the formed composites depends on the conditions of polymerization, in particular on the concentration of composite components and the pH of the reaction environment. Magnetite nanoparticles also significantly affect the electrochemical properties of the polymer phase.

## Materials and methods

### Materials

$\text{FeCl}_2 \cdot 4\text{H}_2\text{O}$ ,  $\text{FeCl}_3 \cdot 6\text{H}_2\text{O}$ , 0.5%  $\text{NH}_3$  solution, acetone, ethanol, tetra(*n*-butyl)ammonium hydroxide (TBAOH), pyrrole (Py), HCl, sodium dodecyl sulphate (SDS), NaCl, acetonitrile (ACN), dichloromethane (DCM) and (*n*- $\text{C}_4\text{H}_9$ ) $_4\text{NClO}_4$  (TBAP) were used as received for the synthesis of  $\text{Fe}_3\text{O}_4$  nanoparticles and its composite with PPy from Aldrich Chemical Co., Milli-Q/Millipore system was used to obtain deionized water with a resistivity of 18.2  $\text{M}\Omega\text{-cm}$ .

### Instrumentation

An AUTOLAB Model 283 Potentiostat/Galvanostat controlled with GPES software (v. 4.9) (EG&G Princeton Applied Research, Oak Ridge, TN, USA) was used in voltammetric measurements in a three-electrode cell. A gold disc electrode with a diameter of 1.5 mm (Bioanalytical Systems Inc., West Lafayette, IN, USA) was used as working electrode. Prior the experiment, the electrode was polished with 0.3  $\mu\text{m}$  Micro Polish Alumina (Buehler Ltd., IL, USA),

rinsed with water and acetone and air dried. In aqueous solvents, an Ag/AgCl/saturated KCl electrode was used as reference electrode. This electrode was separated by a ceramic tip (Bioanalytical Systems Inc.). A platinum foil with an area of approximately  $0.5 \text{ cm}^2$  served as a counter electrode.

TEM images were obtained using a Tecnai G<sup>2</sup> 20 X-TWIN microscope (FEI Company, Hillsboro, Oregon, USA) with an LaB<sub>6</sub> emitter and a high-angle annular dark-field (HAADF) detector operating at 120/200 kV. The accelerating voltage for the electron beam was 200 keV, and the working distance was 10 mm.

A Magna IR 550 Series II spectrometer with a spectral resolution of  $4 \text{ cm}^{-1}$  was used in FT-IR measurements.

Thermogravimetric analysis (TGA) in atmosphere of purged nitrogen ( $0.1 \text{ dm}^3 \text{ min}^{-1}$ ) was performed using a Mettler Toledo Star TGA/DSC system. Two milligram of sample weighing was placed in aluminium pans and heated from 50 to  $1000 \text{ }^\circ\text{C}$  at  $10 \text{ }^\circ\text{C min}^{-1}$ .

The X-ray powder diffraction (XRD) measurements were carried on an Agilent Technologies SuperNova X-ray diffractometer equipped with a Mo microfocused lamp emitting K $\alpha$  radiation with  $\lambda = 0.713067 \text{ nm}$ . A small amount of particles powder was fixed by Paratone<sup>®</sup>N (Hampton Research) oil to nylon loop.

X-ray photoelectron spectroscopy (XPS) was performed using a PHI 5000 VersaProbe (ULVAC-PHI) spectrometer with monochromatic Al K $\alpha$  radiation ( $h\nu = 1486.6 \text{ eV}$ ) from an X-ray source operating at a  $100\text{-}\mu\text{m}$  spot size, 25 W and 15 kV. High-resolution (HR) XPS spectra were collected with a hemispherical analyser using a pass energy of 117.4 eV and an energy step size of 0.1 eV. The X-ray beam was incident on the sample surface at an angle of  $45^\circ$  with respect to the surface normal, and the analyser axis formed an angle of  $45^\circ$  with respect to the surface. Casa XPS software was then used to evaluate the XPS data. Deconvolution of all HR XPS spectra was performed using a Shirley background and a Gaussian peak shape with a 30% Lorentzian character.

The amount of Fe in the solutions obtained after synthesis of Fe<sub>3</sub>O<sub>4</sub>/PPy nanocomposite was measured by atomic absorption spectrometry (AAS). Measurements were performed using an atomic absorption spectrometer iCE 3500 AA Spectro Dual (Thermo Fisher Scientific) equipped with a flame atomizer (burner length: 100 mm). An air–acetylene flame was used for the determination of Fe under optimized conditions (burner height: 7.2 mm, air–C<sub>2</sub>H<sub>2</sub> flow rate:  $1.6 \text{ dm}^3 \text{ min}^{-1}$ ). All absorbance values are the mean values based on three repetitive measurements. The quantitative determination of Fe was carried out by the external calibration graph technique. The limit of detection (LOD) was calculated as 3 times the standard deviation of absorbance signal of blank ( $0.003 \text{ mol dm}^{-3}$  HCl) divided by slope of the regression equation ( $\text{LOD} = 3\text{SD}_{\text{blank}}/a$ ),

while the limit of quantification (LOQ) was calculated as  $10\text{SD}_{\text{blank}}/a$ . The calculated LOD of Fe was  $0.099 \text{ mg dm}^{-3}$ , while LOQ was  $0.332 \text{ mg dm}^{-3}$ .

### Synthesis of Fe<sub>3</sub>O<sub>4</sub>/PPy and Fe<sub>3</sub>O<sub>4</sub>-aggregates@PPy nanocomposite

Fe<sub>3</sub>O<sub>4</sub> nanoparticles were produced according to the modified synthesis first described by Massart [32, 39]. Forty milliliters of NH<sub>3</sub> solution and roughly 1 ml of TBAOH was placed into one round-bottom flask (icy cooled) and deoxygenated by roughly bubbling argon gas for 30 min. Next, about 0.3 g of FeCl<sub>2</sub>·4H<sub>2</sub>O was added to the mixture, still deoxygenated and stirred. In another round-bottom flask, 40 ml of NH<sub>3</sub> solution and 2 ml of TBAOH were heated to  $40 \text{ }^\circ\text{C}$  under continuous argon flow and vigorous stirring by permanent magnet for 30 min. Then, 0.8 g of FeCl<sub>3</sub>·6H<sub>2</sub>O was added to the mixture, still deoxygenated and heated to  $40 \text{ }^\circ\text{C}$  while stirring for 30 min. Finally, the solution from the cooled flask was moved into the flask with FeCl<sub>3</sub>·6H<sub>2</sub>O and the resulting mixture was heated to  $80 \text{ }^\circ\text{C}$  while stirring for 40 min. The resultant dark residue was separated from the solution with a permanent magnet. In the last step, the obtained magnetic nanoparticles were washed a few times using deoxygenated acetone and dried to powder form by evaporator.

Fe<sub>3</sub>O<sub>4</sub>/PPy nanocomposite was synthesized under sonication by chemical polymerization of pyrrole in the presence of the previously synthesized Fe<sub>3</sub>O<sub>4</sub> nanoparticles. In a typical synthesis, 10 mg of Fe<sub>3</sub>O<sub>4</sub> nanoparticles was well dispersed in 10 ml aqueous solution using ultrasonication for 30 min. The colloidal solution of magnetite nanoparticles was acidified to pH 2 with a few drops of 2 M HCl. Next, 70  $\mu\text{l}$  of pyrrole was added dropwise to the above mixture to start the polymerization process. The mixture was ultrasonicated for 4 h at room temperature. Formed black product was collected and washed several times with deionized water. Finally, the samples were dried overnight at  $60 \text{ }^\circ\text{C}$ .

Nanocomposite of magnetite aggregates surrounded by a layer of polypyrrole marked with the abbreviation Fe<sub>3</sub>O<sub>4</sub>-aggregates@PPy was made in the same way, except for that the Fe<sub>3</sub>O<sub>4</sub> nanoparticles were dispersed in aqueous solution acidified to a pH 2 in the presence of 2 mg of SDS in order to minimize their aggregation.

After quantitative separation of the composite from the post-reaction solution, the precipitate was weighed. The weight of the composite deposit allowed to determine the percentage content of its components. The results obtained for various conditions of composite formation are summarized in Table 1.

**Table 1** Composition of Fe<sub>3</sub>O<sub>4</sub> and PPy composites formed under different experimental conditions and PPy shell thickness in Fe<sub>3</sub>O<sub>4</sub>-aggregates@PPy composites

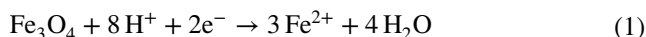
Polymerization conditions	Composite composition PPy/Fe <sub>3</sub> O <sub>4</sub> m/m		Polymer layer thickness <sup>b</sup> in nm	Composite structure
70 μl Py + 2 mg Fe <sub>3</sub> O <sub>4</sub> + 2 mg SDS <sup>a</sup>	1.38 <sup>c</sup>	1.27 <sup>d</sup>	8 ± 2	Fe <sub>3</sub> O <sub>4</sub> -aggregates@PPy
70 μl Py + 5 mg Fe <sub>3</sub> O <sub>4</sub> + 2 mg SDS <sup>a</sup>	1.02 <sup>c</sup>	0.98 <sup>d</sup>	22 ± 8	Fe <sub>3</sub> O <sub>4</sub> -aggregates@PPy
70 μl Py + 10 mg Fe <sub>3</sub> O <sub>4</sub> + 2 mg SDS <sup>a</sup>	0.55 <sup>c</sup>	0.47 <sup>d</sup>	55 ± 11	Fe <sub>3</sub> O <sub>4</sub> -aggregates@PPy
70 μl Py + 20 mg Fe <sub>3</sub> O <sub>4</sub> + 2 mg SDS <sup>a</sup>	0.40 <sup>c</sup>	0.37 <sup>d</sup>	80 ± 25	Fe <sub>3</sub> O <sub>4</sub> -aggregates@PPy
70 μl Py + 10 mg Fe <sub>3</sub> O <sub>4</sub> for 2 h <sup>e</sup>	0.33 <sup>c</sup>	-	-	Fe <sub>3</sub> O <sub>4</sub> /PPy
70 μl Py + 10 mg Fe <sub>3</sub> O <sub>4</sub> for 4 h <sup>e</sup>	0.56 <sup>c</sup>	-	-	Fe <sub>3</sub> O <sub>4</sub> /PPy
70 μl Py + 10 mg Fe <sub>3</sub> O <sub>4</sub> for 6 h <sup>e</sup>	1.35 <sup>c</sup>	-	-	Fe <sub>3</sub> O <sub>4</sub> /PPy

<sup>a</sup>In 10 ml of H<sub>2</sub>O for 4 h<sup>b</sup>From the TEM images<sup>c</sup>Based on the mass of composite<sup>d</sup>From the TGA measurements<sup>e</sup>In 10 ml of H<sub>2</sub>O

## Results and discussion

### Formation and structural characterization of composites

The production of nanocomposites with conducting polymers is commonly achieved through the chemical route in a solution containing the monomer, oxidant and the suspension or nanoparticle colloids as an additional component. Under such conditions, the polymerization process usually takes place both on the surface of nanoparticles and in the solution, although it is difficult to control the morphology of this composite, especially the homogeneity and thickness of the polymer layer. These difficulties can be overcome if the nanoparticles, as one of the components of the composite material, are used simultaneously as oxidant and doping system for the forming polymer. Therefore, nanocomposite formation proceeds through polymerization of pyrrole on the surface of previously synthesized magnetite nanoparticles which are both an oxidant and a component of the composite material. Pang et al. [40] showed that Fe<sup>3+</sup> ions from Fe<sub>3</sub>O<sub>4</sub> nanoparticles are reduced to Fe<sup>2+</sup> ions in a pH range from 1.70 to 3.0. The process of magnetite dissolution can be described by the following reaction:



The Nernst potential of this process can be expressed by the following equation:

$$E_{\text{Fe}_3\text{O}_4/\text{Fe}^{2+}} = E^0_{\text{Fe}_3\text{O}_4/\text{Fe}^{2+}} - RT/2F \ln [\text{Fe}^{2+}]^3 + RT/2F \ln [\text{H}^+]^8 \quad (2)$$

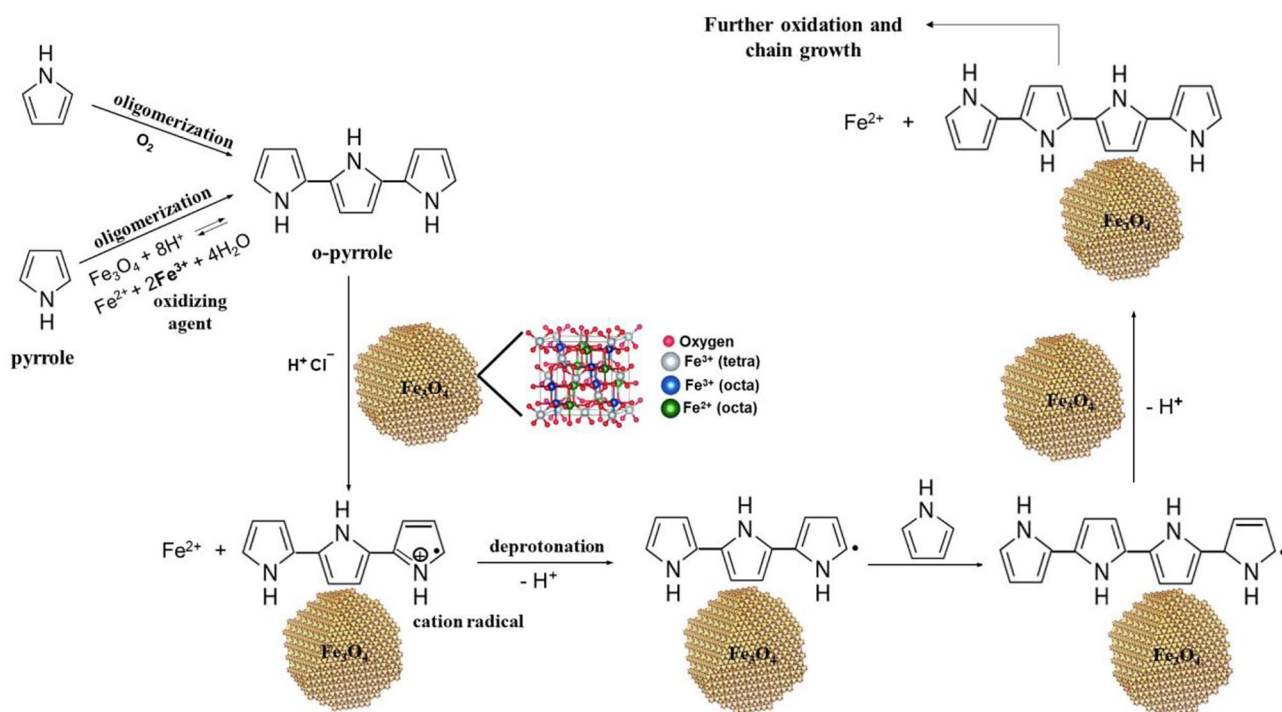
The standard potential  $E^0_{\text{Fe}_3\text{O}_4/\text{Fe}^{2+}}$  in reaction (1) is equal to 1.09 V with respect to the standard hydrogen electrode (SHE) [40]. A higher value of  $E^0_{\text{Fe}_3\text{O}_4/\text{Fe}^{2+}}$  of 0.560 V was reported for magnetite nanoparticle dispersion [40]. The

formal potential of Fe<sub>3</sub>O<sub>4</sub>/Fe<sup>2+</sup> system is significantly lower than the standard potential due to the negative value of the last term ( $RT/2F \ln [\text{H}^+]^8$ ) in Eq. (2). The standard potential of reversible oxidation of pyrrole to pyrrolic cation radicals ( $E^0_{\text{Py}^+/\text{Py}}$ ) was estimated to ~ 1.32 V with respect to the SCE [41]. Even if we consider the low equilibrium concentration of Fe<sup>+2</sup> ions, such differences in the potentials of both redox systems makes the direct oxidation of pyrrole rather unlikely. However, the process of polypyrrole formation takes place with the participation of pyrrole oligomers as intermediate species [42–48]. Pyrrole oligomers can be slowly formed in process of monomer oxidation with Fe<sup>3+</sup> ions produced from partial dissolution of magnetite in acidic solution according to following equation:



The equilibrium of this reaction is shifted significantly towards the undissolved magnetite phase. The total concentration of iron ions in the solution in equilibrium with the solid nanoparticle magnetite was determined by the AAS method. In Table S1 and Fig. S1, the relations between iron ions concentration and pH of solutions are presented for different contact times of the magnetite nanoparticles with the solution. While establishing the equilibrium between the precipitate and iron ions in the liquid phase, the solution was initially stirred with a magnetic stirrer and then left stationary. This limited the transfer of small particles of magnetite into the solution and overestimated the determi-

nation of iron concentration in the liquid phase. The system reaches equilibrium very slowly. The concentration of iron ions in the solution ranges from ca 0.10 to 50 mg dm<sup>-3</sup> with a change in pH from 3.5 to 2, respectively. Fe<sup>3+</sup> ions formed



**Scheme 1** Schematic illustration of Fe<sub>3</sub>O<sub>4</sub>-assisted pyrrole polymerization

as a result of magnetite dissolution may participate in the process of pyrrole oligomerization, initiating the polymerization process. Traces of pyrrole oligomers can be also found in solid face exposed to light and air [49]. The oligomerization process accelerates in water, particularly in the presence of acids [50, 51].

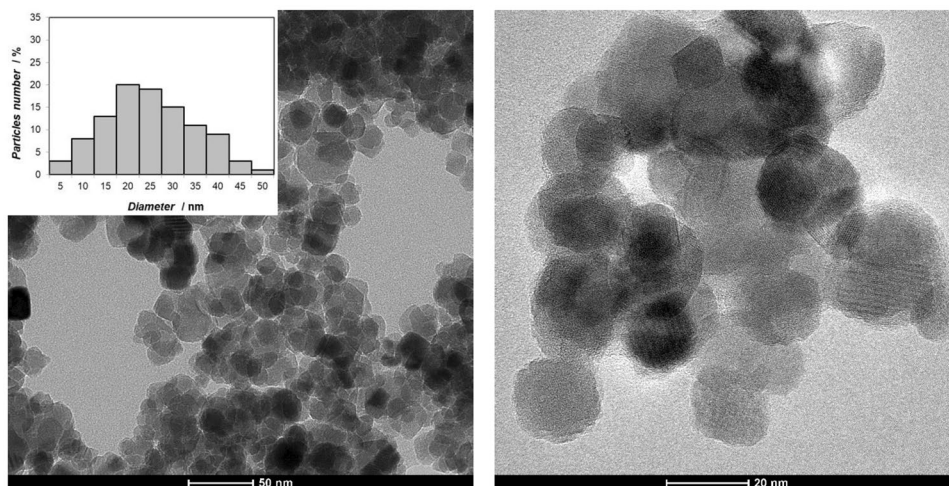
The oxidation potentials of the pyrrole oligomeric species shifts toward less positive potentials in comparison to the oxidation potential of monomer. The magnitude of this shift depends on the number of pyrrole units in the oligomeric structure [52, 53]. For example, the PPy oxidation potential is approximately 400 mV less positive than the pyrrole oxidation potential [52]. Therefore, these oligomeric structures can replace isolated pyrrole molecules in the polymerization process at the surface of magnetite nanoparticles as is schematically described in Scheme 1. For simplicity, we show only the oligomeric form composed of three monomeric units. A similar behaviour was reported for the process of C<sub>60</sub>@PPy composite formation in which fullerene was used as an oxidation agent in a pyrrole oligomer oxidation process [52]. Also in this case, the potential sequence of pyrrole oxidation and fullerene reduction clearly indicates that pyrrole cannot be directly oxidized by fullerene C<sub>60</sub>.

To confirm these results, we carried out the synthesis of this nanocomposite in an aqueous solution containing only pyrrole and magnetite nanoparticles and in an acidified hydrochloric acid aqueous solution with different pH values (pH=2, 3 and 5) containing pyrrole and magnetite

nanoparticles. We found that this composite did not form in the neutral solution (without acidification). Furthermore, in aqueous solution acidified to pH 5, the yield of composite formation was very low. Lowering the pH resulted in significantly higher polymerization yields and composite formation. Thus, the fundamental parameter for the formation of this type of material is pH which needs to be set accordingly to allow oxidation of the pyrrole by Fe<sub>3</sub>O<sub>4</sub>. Transmission electron microscopy (TEM) and electrochemical measurements indicated that a pH of 2 was most effective at facilitating polymer formation on the surface of Fe<sub>3</sub>O<sub>4</sub> nanoparticles. Hence, all further studies were carried out with the nanocomposite created in an aqueous solution with pH 2.

We used transmission electron microscopy to characterize the morphology and size of Fe<sub>3</sub>O<sub>4</sub> nanoparticles and their nanocomposites with polypyrrole. They have a near-spherical shape. Diagram of size distribution of magnetite nanoparticles (inset in Fig. 1) shows a relatively broad range of nanoparticle diameters from 5 to 50 nm. These particles show tendency to form agglomerates (Fig. 1). The Fe<sub>3</sub>O<sub>4</sub>/PPy nanocomposite morphology shows that the polypyrrole film is formed unevenly on the surface of the magnetite nanoparticles (Fig. 2a). Addition of a surfactant during the synthesis yields a smoother and more uniform layer of the conducting polymer covering the magnetite surface, creating a Core-shell nanocomposite (Fig. 2b). However, these Core-shell particles exhibit tendency to aggregation after separation from the solution. Based on the TEM images, the

**Fig. 1** TEM images of  $\text{Fe}_3\text{O}_4$  nanoparticles at different magnifications. The inset shows a size distributions of magnetite nanoparticles



thickness of the shell of polymeric layer coating magnetite nanoparticles was estimated. The relevant data are summarized in Table 1 for materials formed in solution containing different mass ratio of magnetite to pyrrole.

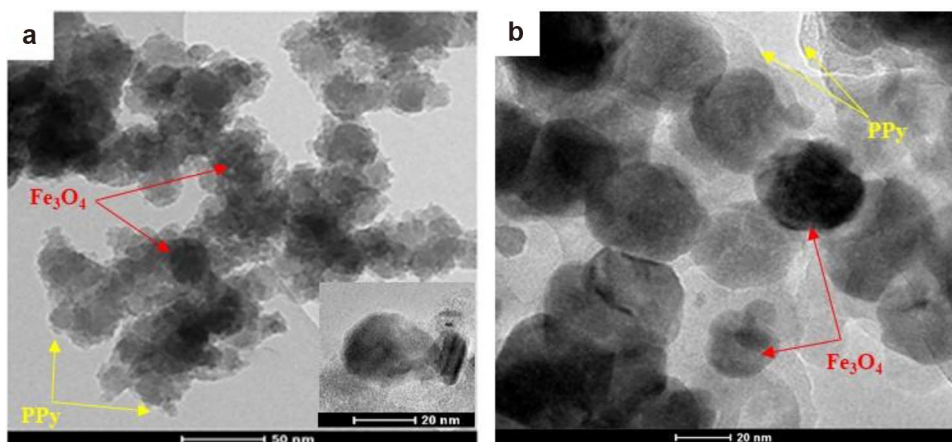
X-ray diffraction was applied to characterize the crystal structure of the chemical components of the formed nanocomposite (Fig. 3). The diffractograms show several significant diffraction peaks corresponding to pure magnetite nanoparticles, located at  $2\theta = 13.5^\circ$ ,  $16.0^\circ$ ,  $19.0^\circ$ ,  $23.5^\circ$ ,  $25.0^\circ$  and  $27.0^\circ$ , which correspond to (220), (311), (400), (422), (511) and (440) Bragg reflections, respectively (Fig. 3a). Pure polypyrrole is amorphous and therefore exhibits only a broad peak at  $2\theta < 15^\circ$  in the XRD pattern of the  $\text{Fe}_3\text{O}_4/\text{PPy}$  nanocomposite (Fig. 3b).

The composition of the  $\text{Fe}_3\text{O}_4/\text{PPy}$  nanocomposite was also confirmed by FT-IR spectroscopy (Fig. 4). The spectrum of  $\text{Fe}_3\text{O}_4$  nanoparticles (Fig. 4a) reveals an absorption band at  $590\text{ cm}^{-1}$ , which corresponds to the vibration of the Fe–O stretching band [54]. In the spectrum of pure polypyrrole (Fig. 4b), the characteristic bands at  $930$  and  $1050\text{ cm}^{-1}$  are assigned to out-of-plane and in-plane vibrations of the

C–H bond, respectively [35, 54]. The signals at  $1190$  and  $1310\text{ cm}^{-1}$  are assigned to C–N stretching while the peaks at  $1465$  and  $1555\text{ cm}^{-1}$  are due to stretching of the C=C bands in the pyrrole ring [35, 54, 55]. The spectrum of  $\text{Fe}_3\text{O}_4/\text{PPy}$  nanocomposite (Fig. 4c) clearly shows characteristic peaks of both  $\text{Fe}_3\text{O}_4$  nanoparticles and pure polypyrrole. However, the bands at  $1310$  and  $1465\text{ cm}^{-1}$  are not observed in composite. This proves the existence of interactions between the magnetite and the polypyrrole layer. It is also indicated by small shifts of some absorption bands towards higher wave numbers in the spectrum of the composite in relation to the spectra obtained for its components.

The surface chemical compositions of the prepared materials were investigated using XPS analysis. In Fig. 5, the XPS spectra of magnetite nanoparticles are presented. The Fe  $2p_{3/2}$  spectrum (Fig. 5a) shows “multiplet splitting” states. In magnetite, iron exists in two oxidation states, namely  $\text{Fe}^{2+}$  and  $\text{Fe}^{3+}$ . The  $\text{Fe}^{2+}$  ions are octahedrally coordinated with oxygen. The  $\text{Fe}^{3+}$  centres are distributed over both octahedral and tetrahedral sites. The binding energy peak at  $709.92\text{ eV}$  is related to  $\text{Fe}^{2+}$  with a corresponding

**Fig. 2** TEM images of **a**  $\text{Fe}_3\text{O}_4/\text{PPy}$  nanocomposite formed in 10 ml of solution containing 10 mg  $\text{Fe}_3\text{O}_4$  and  $70\text{ }\mu\text{l}$  Py, and **b**  $\text{Fe}_3\text{O}_4$ -aggregates@PPy nanocomposite formed in the same solution containing additionally 2 mg of SDS



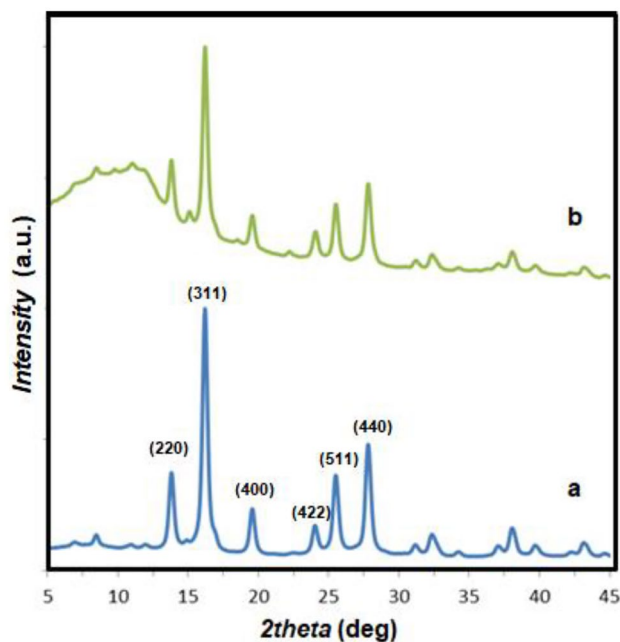
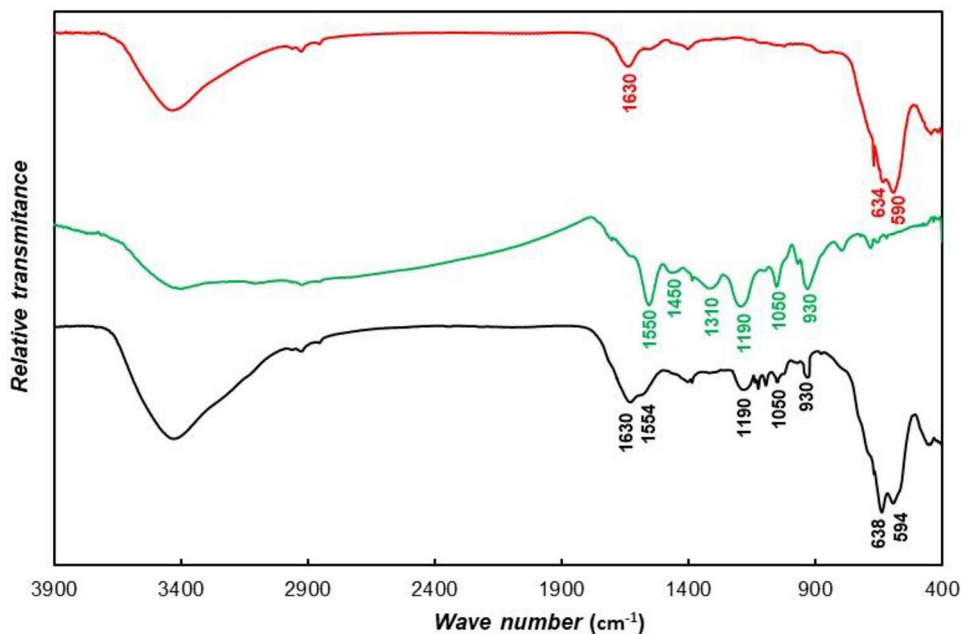


**Fig. 3** Typical XRD diffractograms of (a)  $\text{Fe}_3\text{O}_4$  nanoparticles and (b)  $\text{Fe}_3\text{O}_4/\text{PPy}$  nanocomposite

satellite at 708.53 eV. The  $\text{Fe}^{3+}$  octahedrally located species exhibit a binding energy of 711.09 eV. The other two peaks are derived from  $\text{Fe}^{3+}$  tetrahedral species at 712.3 eV and 713.63 eV with a  $\text{Fe}^{3+}$  satellite peak at 715.31 eV [56, 57]. The oxygen functional groups were observed in the O 1s spectrum (Fig. 5b) which can be fit to four peaks with binding energies of 529.98 eV, 531.48 eV, 533.04 eV and 534.38 eV. The peak at 529.98 eV is attributed to the lattice

**Fig. 4** FT-IR spectra of (a)  $\text{Fe}_3\text{O}_4$  nanoparticles, (b) PPy chemically synthesized with  $\text{FeCl}_3$  as oxidant and (c)  $\text{Fe}_3\text{O}_4/\text{PPy}$  nanocomposite formed in 10 ml of solution containing 10 mg  $\text{Fe}_3\text{O}_4$  and 70  $\mu\text{l}$  Py



oxygen in  $\text{Fe}_3\text{O}_4$ . The second signal at 531.48 eV is related to hydroxyl groups present at the magnetite surface. The 533.04 eV binding energy is probably attributed to the traces of TBAOH which was used as a surfactant during the synthesis. The relatively low intensity peak at 534.38 eV represents the physically adsorbed  $\text{H}_2\text{O}$  [56–59].

The XPS analysis to identify the chemical compositions of the  $\text{Fe}_3\text{O}_4/\text{PPy}$  nanocomposite is shown in Fig. 6. Here, the XPS spectra for Fe 2p and O 1s are images obtained for pure magnetite nanoparticles (see Fig. 6a, b) while the C 1s XPS spectrum shows functional groups such as C=C ( $\text{sp}^2$  carbon) at 284.67 eV, C–C ( $\text{sp}^3$  carbon) at 285.62 eV, C–O at 286.59 eV, C=O and C–N at 287.55 eV, O=C–O at 288.63 eV,  $\pi$  electrons in the aromatic rings at 289.8 eV and  $\pi$ - $\pi^*$  conjugation at 291.65 eV (Fig. 6c) [37, 60–62]. These species are due to polypyrrole film in the composite material. An additional confirmation for the existence of polypyrrole in the  $\text{Fe}_3\text{O}_4$ -aggregates@PPy nanocomposite is the N 1s spectrum (Fig. 6d) which is composed of four components. The major signal at a binding energy of 400.44 eV is related to amine nitrogen (N–H) while the signal at 398.53 eV corresponds to imine nitrogen species (C=N). The presence of this latter peak indicates that polypyrrole is produced in its over-oxidized state. Two additional peaks at 401.67 eV and 403.17 eV are assigned to the positively charged nitrogen C–N $^+$  and C=N $^+$ , respectively [63].

The TGA curves of  $\text{Fe}_3\text{O}_4$  nanoparticles,  $\text{Fe}_3\text{O}_4/\text{PPy}$  nanocomposite, and pure polypyrrole in the argon atmosphere are shown in Fig. 7. Magnetite nanoparticles are thermally stable in the studied temperature range (curve 1 in Fig. 7). In contrast, polypyrrole exhibits two stages of thermal degradation (curve 2 in Fig. 7). The first decrease

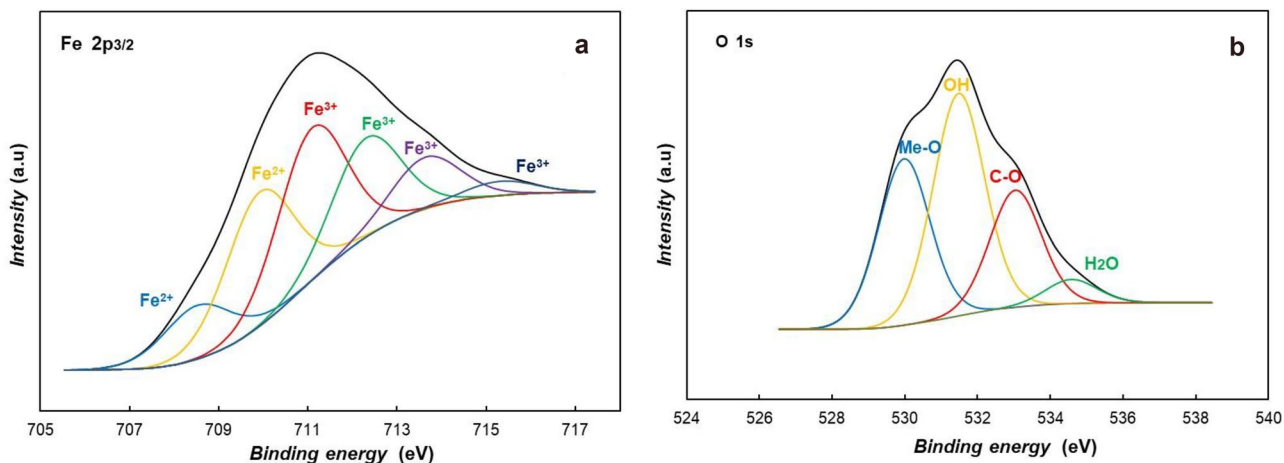


**Fig. 5** X-ray photoelectron spectra of Fe<sub>3</sub>O<sub>4</sub> nanoparticles. The binding energy regions are **a** Fe 2p<sub>2/3</sub> and **b** O 1s electrons

in weight occurs below 100 °C and can be attributed to a loss of water, while the second occurs in the temperature range from 200 to 450 °C and is related to the thermal degradation of the polymer chain. The weight loss of pure

polypyrrole reached about 90% at ca. 450 °C. The behaviour of the composite under thermogravimetric conditions is very surprising. The first loss of weight below 100 °C is associated with the removal of water traces. At higher

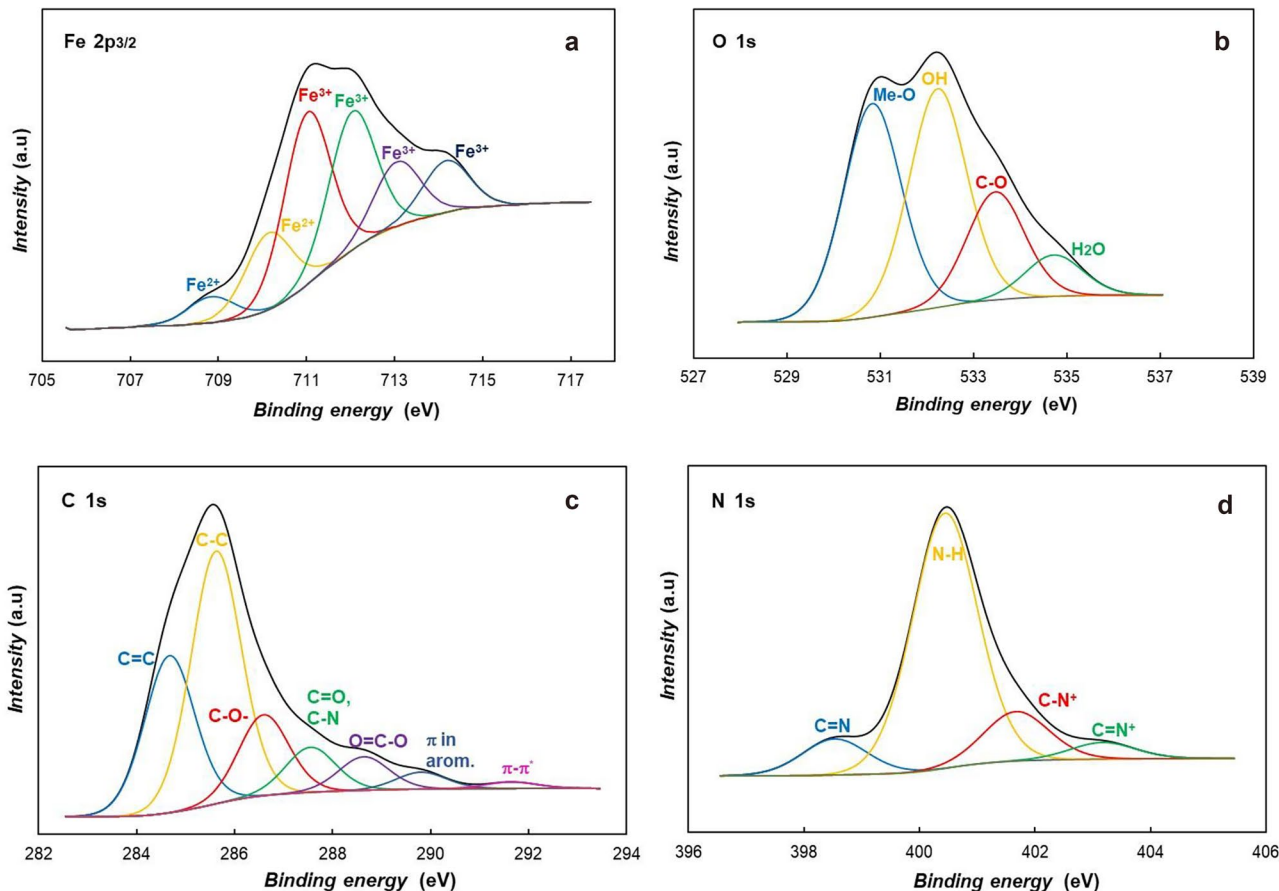
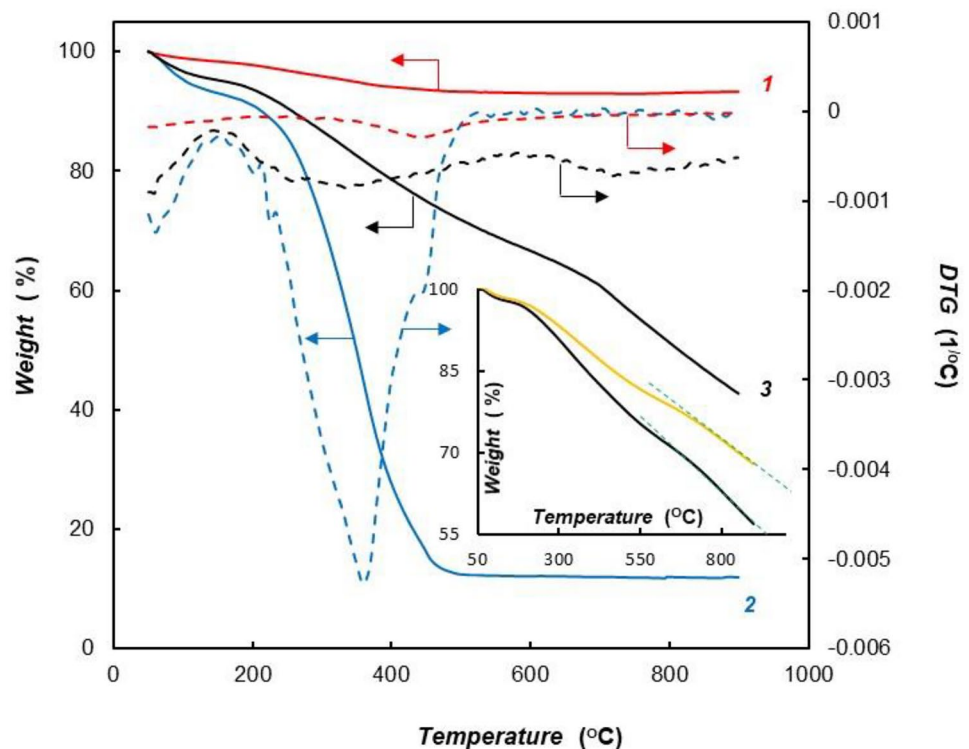


**Fig. 6** X-ray photoelectron spectra of Fe<sub>3</sub>O<sub>4</sub>-aggregates@PPy nanocomposite formed in 10 ml of solution containing 10 mg Fe<sub>3</sub>O<sub>4</sub>, 70 μl Py and 2 mg SDS. The binding energy regions are **a** Fe 2p<sub>2/3</sub>, **b** O 1s, **c** C 1s and **d** N 1s electrons

**Fig. 7** TGA (solid lines) and DTG (dashed lines) curves of (1)  $\text{Fe}_3\text{O}_4$  nanoparticles, (2) pure PPy and (3)  $\text{Fe}_3\text{O}_4$ /PPy nanocomposite recorded in an argon atmosphere. Composite was formed in 10 ml of solution containing 10 mg  $\text{Fe}_3\text{O}_4$  and 70  $\mu\text{l}$  Py. Inset shows TGA measurements of  $\text{Fe}_3\text{O}_4$ /PPy nanocomposite formed in solutions containing 10 mg  $\text{Fe}_3\text{O}_4$  and 70  $\mu\text{l}$  Py (black line) and 10 mg  $\text{Fe}_3\text{O}_4$  and 35  $\mu\text{l}$  Py (yellow line)

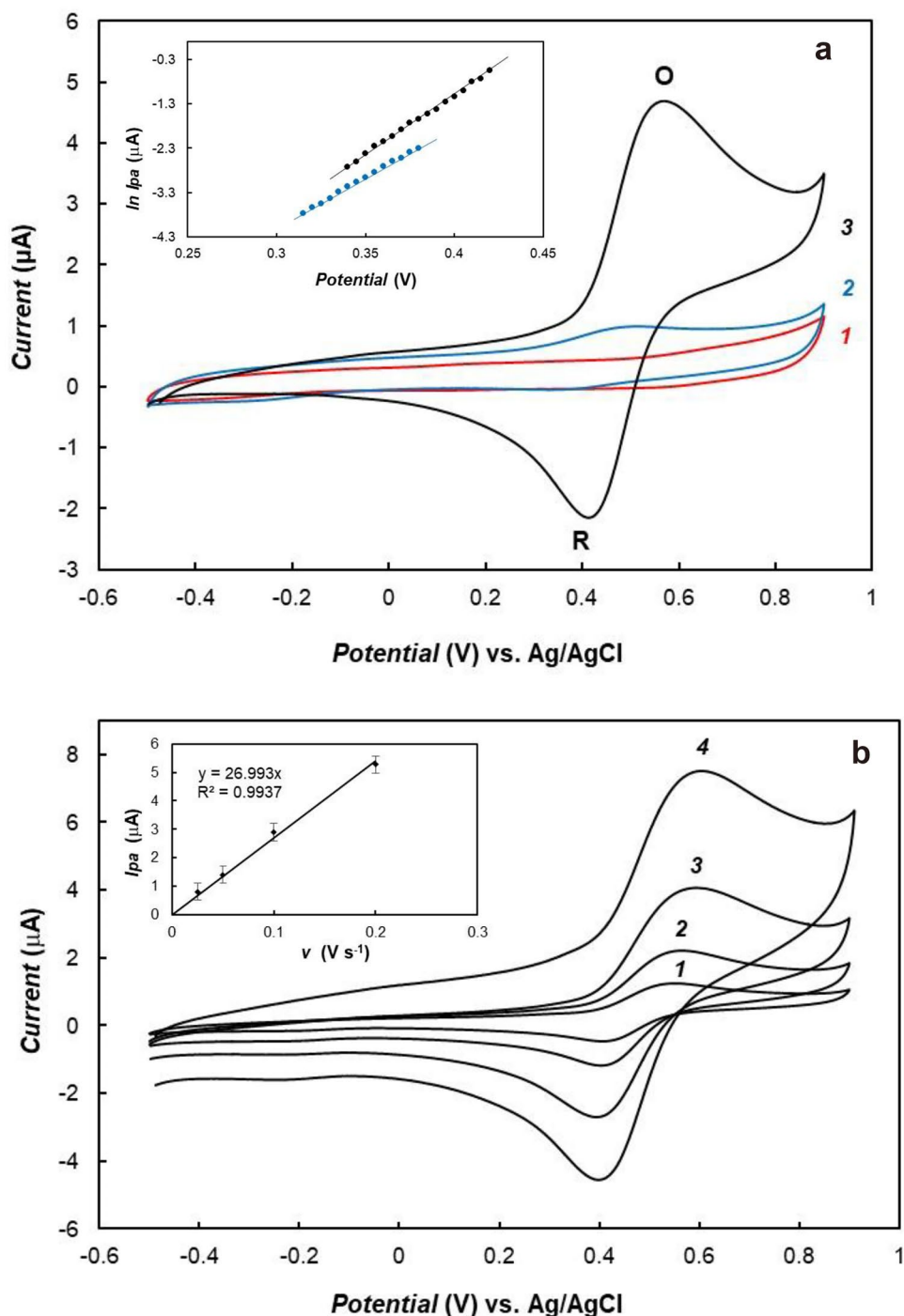


temperatures, a thermal decomposition of PPy is observed. In the case of composite, the temperature range of polymer degradation is much wider in comparison to pure PPy degradation. At temperature higher than 700 °C, the additional inflection associated with the weight loss of the composite is observed in the thermogravimetric curves. The inset in Fig. 7 shows thermogravimetric curves recorded for composites containing the same amount of  $\text{Fe}_3\text{O}_4$  and different mass of PPy. The mass changes in temperature range from 200 to 700 °C depend on the amount of PPy within the composite. However, the mass of decomposed material at temperature exceeding 700 °C is the same in both cases. It is very likely that partial reduction of magnetite particles during polymer deposition results in lowering thermal stability of magnetite nanoparticles and their decomposition. Similar thermogravimetric curves were recorded for Core-shell  $\text{Fe}_3\text{O}_4$ @PPy nanoparticles formed by pyrrole oxidation with  $(\text{NH}_4)_2\text{S}_2\text{O}_8$  at magnetite nanoparticles [64]. In three-component nanocomposite PPy/ $\text{Fe}_3\text{O}_4$ /Ag such unexpected thermogravimetric behaviour in high temperature range was also observed [65]. Based on the thermogravimetric curves, the ratio of polymeric mass to mass of magnetite in the composite material was estimated. Results of this calculation are summarized in Table 1. There is a good agreement between the quantitative composition of the composites obtained on the basis of thermogravimetric analysis and the weight of the cast materials.

## Electrochemical properties

A gold electrode coated with magnetite-containing materials was fabricated using a drop-coating method. The stable and homogeneous dispersions of  $\text{Fe}_3\text{O}_4$  nanoparticles or their nanocomposite with polypyrrole were obtained by sonication of the studied material in dichloromethane solution. Twenty microliters of a mixture containing 1.5 mg of magnetite-containing material in 1 ml of solution was dropped onto the surface of the Au electrode, and the solvent was evaporated. This nanoparticle-modified gold electrode was characterized by cyclic voltammetry. In Fig. 8a, the voltammetric behaviour of a thin film of the  $\text{Fe}_3\text{O}_4$ -aggregates@PPy nanocomposite and, for comparison, voltammograms of magnetite nanoparticles layer and pure polypyrrole film deposited at the gold electrode surface in the aqueous solution containing 0.1 M NaCl as supporting electrolyte are shown. In the case of pure PPy layer, 10  $\mu\text{l}$  of dispersion containing 1.5 mg of PPy in 1 ml of solution was dropped onto the surface of the Au electrode, and the solvent was evaporated. Therefore, the mass of PPy deposited at the electrode surface and within the composite was the same. The  $\text{Fe}_3\text{O}_4$ -aggregates@PPy nanocomposite is electrochemically active at positive potentials due to polypyrrole electrochemical oxidation, while pure magnetite was passive throughout the studied potential range. The results clearly show the reversible electrochemical behaviour of composite with distinct oxidation (O) and reduction (R) peaks. The polymer phase oxidation is a

**Fig. 8** Cyclic voltammograms of **a**  $\text{Fe}_3\text{O}_4$  nanoparticles (curve 1), pure PPy (curve 2) and  $\text{Fe}_3\text{O}_4$ -aggregates@PPy nanocomposite formed in 10 ml of solution containing 10 mg  $\text{Fe}_3\text{O}_4$ , 70  $\mu\text{l}$  Py and 2 mg SDS (curve 3) recorded at a potential sweep of  $0.1 \text{ V s}^{-1}$ . The mass of PPy deposited at the electrode surface (curve 2) and within the composite (curve 3) was the same and equal to  $850 \mu\text{g cm}^{-2}$ . Studied materials have been deposited at the electrode surface by a drop-coating method. Inset shows the  $\ln i$ - $E$  relationship for the first 10% of the PPy oxidation peak high for electrode covered with  $\text{Fe}_3\text{O}_4$ -aggregates@PPy nanocomposite (black line) and pure PPy (blue line). **b**  $\text{Fe}_3\text{O}_4$ -aggregates@PPy nanocomposite recorded for different potential sweeps of (1) 0.025, (2) 0.05, (3) 0.1 and (4)  $0.2 \text{ V s}^{-1}$  at the gold electrode in aqueous solution containing 0.1 M NaCl as supporting electrolyte. The inset in panel **b** shows the dependence of the polypyrrole oxidation peak current on the sweep rate



complex process that involves electron transfer between the electrode and the polymer, electron transport through the polymeric phase, transport of the counterions from the electrolyte to the polymeric phase and within the polymer material to maintain the neutral charge. These processes are also accompanied by structural changes of the polymeric phase and solvent swelling. Chemically formed pristine polypyrrole deposited at the electrode surface by the drop-coating method usually shows low efficiency of pyrrole oxidation in

relation to the mass of material deposited on the electrode surface and low reversibility of electrode processes under cyclic polarization conditions [14, 66–68]. The polypyrrole oxidation current is much higher for the composite compared to the electrode coated with the pristine polymer. This effect is related to the nanostructured morphology of composite. A thin layer of polypyrrole covering the surface of magnetite nanoparticles causes the doping process to take place in a larger amount of polymeric material. Nanostructured

morphology is responsible for the fast counterion transport within the polymeric phase. Also, the reversibility of the charge transfer processes is significantly enhanced with the  $\text{Fe}_3\text{O}_4$ -aggregates@PPy nanocomposite. The rate of the PPy electro-oxidation (peak O in Fig. 8a) can be expressed by the slope of the relation between the logarithm of the oxidation current and the potential in the potential range of the oxidation peak formation (approximately the first 10% of the oxidation peak high). The value of this slope is significantly larger in the case of the  $\text{Fe}_3\text{O}_4$ -aggregates@PPy nanocomposite in comparison to this one obtained for the electrode modified with pure chemically formed PPy (inset in Fig. 8a). This effect is probably related to the nanostructured morphology of composite which enables faster transport of the supporting electrolyte ions into the polymer phase, accelerating the process of polypyrrole oxidation. Furthermore, the peak current of polypyrrole oxidation linearly depends on the sweep rate over the range  $0.025$ – $0.2 \text{ V s}^{-1}$  (Fig. 8b). This behaviour is characteristic of electrode processes in which a solid electroactive phase is deposited onto the surface of the electrode and indicates the rapid transport of counter ions from the solution into the polymer phase [69, 70].

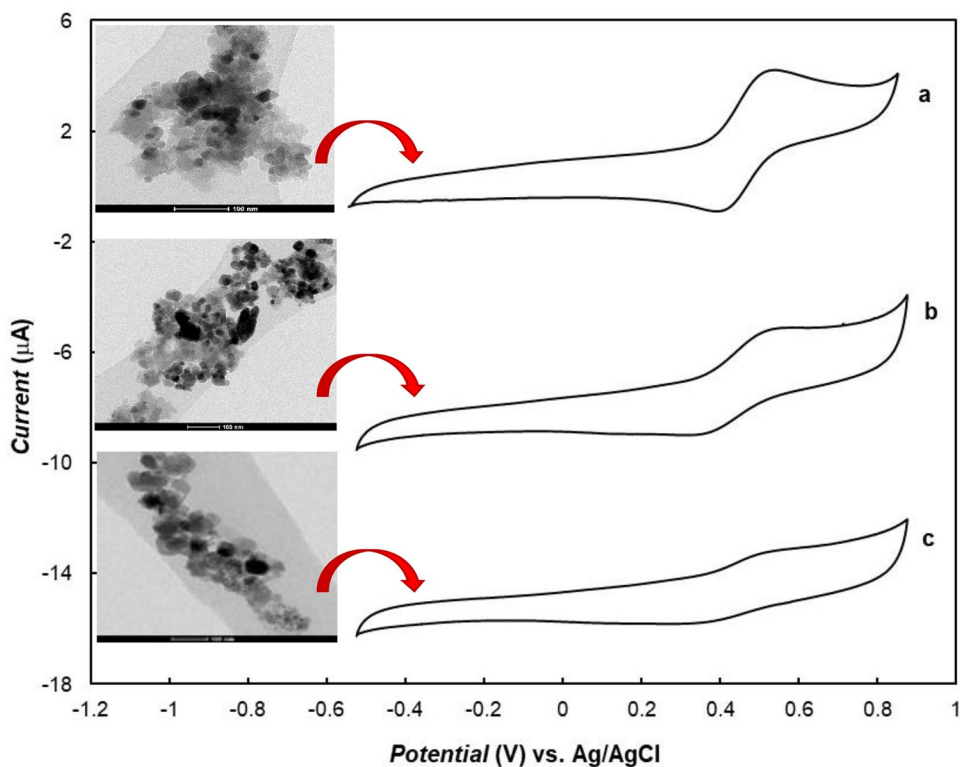
As mentioned above, the solution's pH was the crucial factor determining the formation of the  $\text{Fe}_3\text{O}_4$ /PPy nanocomposite as it determines the pyrrole polymerization process and thus the formation of this nanocomposite, thereby enabling both the reduction of magnetite nanoparticles and the oxidation of the pyrrole. In order to elucidate the role of

pH, cyclic voltammograms for  $\text{Fe}_3\text{O}_4$ /PPy nanocomposites formed in aqueous solutions of different pH values were recorded (Fig. 9). While the amount of magnetite in the nanocomposite formation solution was unaffected by pH, lower pH generally resulted in higher voltammetric currents, creating offsets between the different curves. This effect is related to the lower efficiency of the polymerization process as pH increases. Through TEM images we could confirm hypothesis regarding the effect of pH on the efficiency of the polymerization process and the voltammetric response of composites (Fig. 9).

Both the polymerization time and component concentration also significantly affected the electrochemical properties and the morphology of the obtained nanocomposite. More specifically, an increase in polymerization time and pyrrole concentration led to the formation of thicker polymer layers in the nanocomposite structure and therefore higher currents corresponding to the redox process of the polymer film. In contrast, a decrease in magnetite concentration during the synthesis resulted in a better separation of the nanoparticles. Nevertheless, better separation of nanoparticles still did not lead to the formation of a Core-shell system, however (Fig. 10).

Voltammetric behaviour of composites formed in solution containing different amount of magnetite nanoparticles is shown in Fig. 11. Voltammograms were recorded for the same mass of composite deposited at the electrode surface. Current density of the PPy oxidation peak

**Fig. 9** Cyclic voltammograms of  $\text{Fe}_3\text{O}_4$ /PPy nanocomposite synthesized in 10 ml of solution containing 10 mg  $\text{Fe}_3\text{O}_4$  and 70  $\mu\text{l}$  Py at pH: **a** 2, **b** 3 and **c** 5, recorded at the gold electrode in aqueous solution containing 0.1 M NaCl as supporting electrolyte. Composites have been deposited at the electrode surface by a drop-coating method. Insets show the TEM images of the  $\text{Fe}_3\text{O}_4$ /PPy nanocomposite



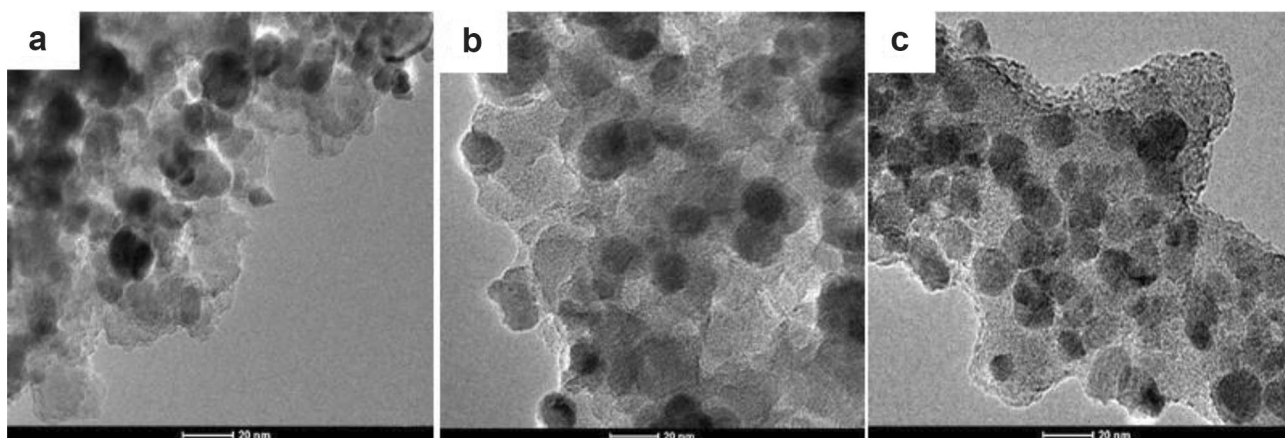


**Fig. 10** TEM images of  $\text{Fe}_3\text{O}_4/\text{PPy}$  nanocomposite synthesized for 4 h at room temperature in 10 ml of solution containing 70  $\mu\text{l}$  of Py and a 10 mg, **b** 5 mg and **c** 2 mg of  $\text{Fe}_3\text{O}_4$

correlates with the amount of magnetite in the solution used for the composite synthesis. An increase in the mass of magnetite leads to an increase in the amount of the polymer phase formed in the composite. Such behaviour

also indicates that  $\text{Fe}_3\text{O}_4$  particles act as an oxidant in the pyrrole polymerization. Increase of the amount of polymeric phase in the composite also results in the polypyrrole electro-oxidation potential towards more positive

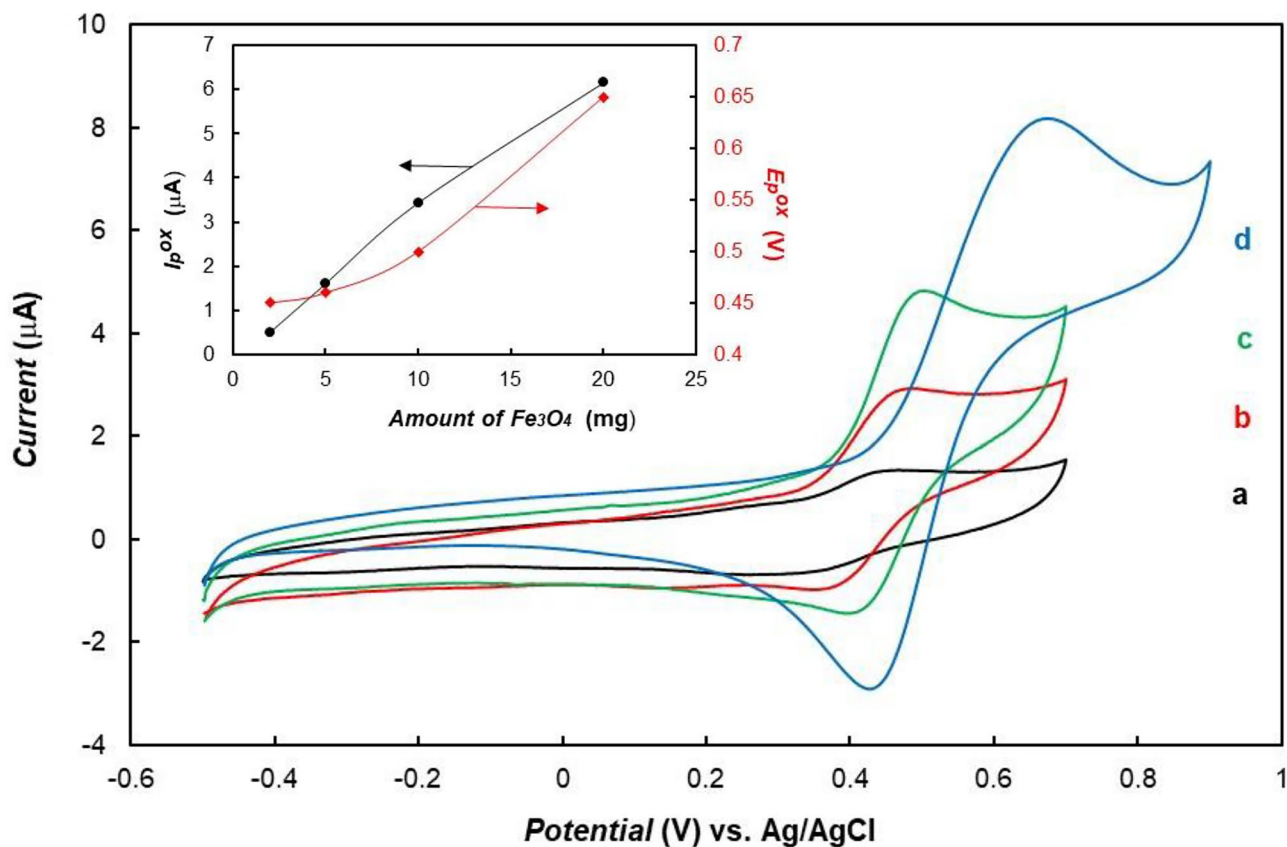
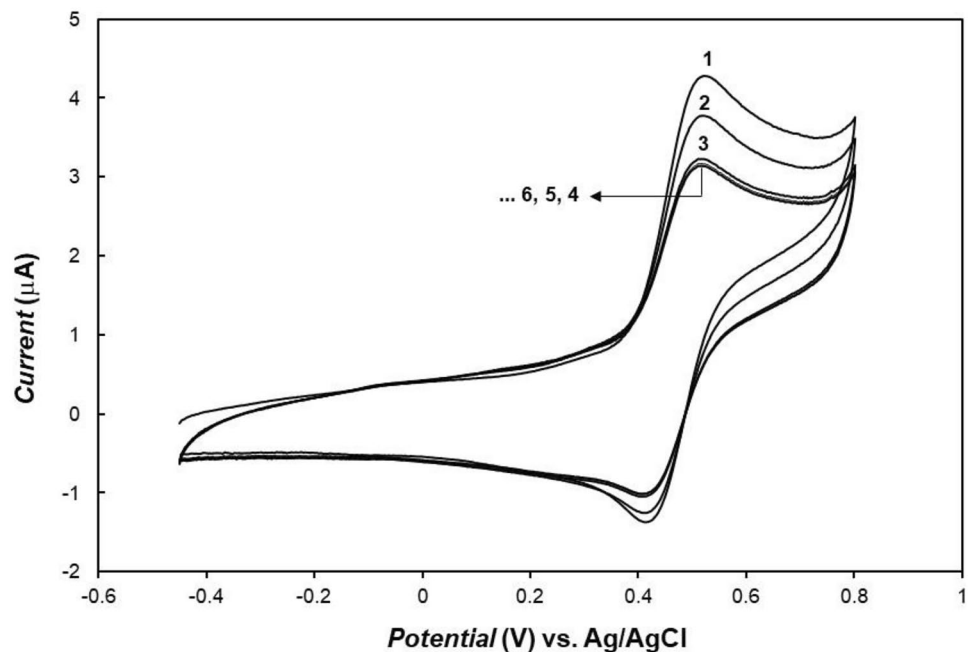


**Fig. 11** Cyclic voltammograms of  $\text{Fe}_3\text{O}_4/\text{PPy}$  nanocomposite synthesized in 10 ml of solution containing 70  $\mu\text{l}$  Py and (a) 2 mg  $\text{Fe}_3\text{O}_4$ , (b) 5 mg  $\text{Fe}_3\text{O}_4$ , (c) 10 mg  $\text{Fe}_3\text{O}_4$  and (d) 20 mg  $\text{Fe}_3\text{O}_4$  recorded at the gold electrode in aqueous solution containing 0.1 M NaCl as sup-

porting electrolyte. Sweep rate was 0.1  $\text{V s}^{-1}$ . Composites have been deposited at the electrode surface by a drop-coating method. Inset shows dependence of the anodic peak current and potential on the amount of  $\text{Fe}_3\text{O}_4$  in the composite

**Fig. 12** Multicyclic voltammogram of  $\text{Fe}_3\text{O}_4$ -aggregates@PPy nanocomposite formed in 10 ml of solution containing 10 mg  $\text{Fe}_3\text{O}_4$ , 70  $\mu\text{l}$  Py and 2 mg SDS recorded at a potential sweep of  $0.1 \text{ V s}^{-1}$ . Composite has been deposited at the electrode surface by a drop-coating method



potentials (inset in Fig. 11). This effect is probably related to the uncompensated ohmic resistance.

Composites deposited at the electrode surface by a drop-coating method exhibit relatively stable mechanical properties. The modified electrode can be transfer from one solution to another without loss of deposit from the electrode surface. The electrochemical stability upon cyclic charging/discharging of  $\text{Fe}_3\text{O}_4$ -aggregates@PPy nanocomposite was investigated under multicyclic voltammetric conditions. In Fig. 12, an exemplary multicyclic voltammograms recorded for the electrode coated with  $\text{Fe}_3\text{O}_4$ -aggregates@PPy in solution containing 0.1 M NaCl is shown. The composite shows relatively stable electrochemical properties. After decrease of PPy-involved currents in the first three voltammetric cycles, the composite achieve stable electrochemical properties. Starting from the fourth cycle, the voltammetric cycles remain virtually unchanged.

## Conclusions

Magnetic  $\text{Fe}_3\text{O}_4$  nanoparticles with polypyrrole nanocomposite was prepared using a new chemical polymerization technique during which  $\text{Fe}_3\text{O}_4$  was used as oxidant for the polymerization process. Nanocomposite in the form of a layer PPy deposited on the surface of the agglomerated  $\text{Fe}_3\text{O}_4$  nanoparticles. Adding a surfactant to the synthesis resulted in the  $\text{Fe}_3\text{O}_4$ -aggregates@PPy Core-shell nanocomposite structures formation. The amount of polymeric material deposited on the magnetite surface depends on the pH of

the solution, the polymerization time and the concentration of the polymerization monomer. Despite their rather different morphologies, these materials possess many similar properties. The IR, XRD and XPS analyses suggested an interaction between the polypyrrole film and the magnetic  $\text{Fe}_3\text{O}_4$  nanoparticles. Furthermore, results of TGA measurements showed that the thermal stability of the polymeric material in the nanocomposite was enhanced compared to pure polypyrrole. The main focus of our study was to examine the electrochemical properties of  $\text{Fe}_3\text{O}_4$ -aggregates@PPy composites, which showed a highly stable and reversible electrochemical behaviour. The highly developed surface, on the other hand, ensures high current density associated with the electrochemical processes involving polypyrrole. Polypyrrole incorporated into composite with magnetite nanoparticles exhibits enhanced electrochemical properties in comparison to pure polypyrrole film deposited at the electrode surface. In case of composite, both polymer material oxidation current and rate of charge transfer are much larger than that of the pure polymer. Despite the relatively significant contribution of non-conductive magnetite nanoparticles in the composite, the material exhibits good electronic conductivity in the potentials range of polypyrrole oxidation.

Polypyrrole and polypyrrole-based materials are frequently used as a component of charge storage devices [71–74]. High polypyrrole-involved oxidation current, fast charge transfer rate and good conductivity make  $\text{Fe}_3\text{O}_4$ -aggregates@PPy compositions particularly useful for electrical charge storage. In this case, however, it is necessary to improve the electrochemical durability of the composite under cyclic charging and discharging.

**Supplementary Information** The online version contains supplementary material available at <https://doi.org/10.1007/s10008-023-05554-2>.

**Acknowledgements** We also thanks for Dr. Agnieszka Wilczewska for assistance in thermogravimetric analysis and to Dr. Alina Dubis for assistance in IR spectroscopy studies.

**Funding** This research was funded by Polish National Science Centre grant No. 2020/04/X/ST5/00702 (K.W.).

## Declarations

**Conflict of interest** The authors declare no competing interests.

**Open Access** This article is licensed under a Creative Commons Attribution 4.0 International License, which permits use, sharing, adaptation, distribution and reproduction in any medium or format, as long as you give appropriate credit to the original author(s) and the source, provide a link to the Creative Commons licence, and indicate if changes were made. The images or other third party material in this article are included in the article's Creative Commons licence, unless indicated otherwise in a credit line to the material. If material is not included in the article's Creative Commons licence and your intended use is not permitted by statutory regulation or exceeds the permitted use, you will need to obtain permission directly from the copyright holder. To view a copy of this licence, visit <http://creativecommons.org/licenses/by/4.0/>.

## References

- Shi Y, Pan L, Liu B, Wang Cui Y, Bao Z, Yu G (2014) Nanostructured conductive polypyrrole hydrogels as high-performance, flexible supercapacitor electrodes. *J Mater Chem A* 2:6086–6091. <https://doi.org/10.1039/C4TA00484A>
- Xue M, Li F, Chen D, Yang Z, Wang X, Ji J (2016) High-oriented polypyrrole nanotubes for next-generation gas sensor. *Adv Mater* 28:8265–8270. <https://doi.org/10.1002/adma.201602302>
- Jeon SS, Kim C, Ko J, Im SS (2011) Spherical polypyrrole nanoparticles as a highly efficient counter electrode for dye-sensitized solar cells. *J Mater Chem* 21:8146–8151. <https://doi.org/10.1039/C1JM10112A>
- Li J, Hu Y, Liang X, Chen J, Zhong L, Liao L, Jiang L, Fuchs H, Wang W, Wang Y, Chi L (2020) Micro organic light emitting diode arrays by patterned growth on structured polypyrrole. *Adv Opt Mater* 8:1902105. <https://doi.org/10.1002/adom.201902105>
- Tabačiarová J, Mičušík M, Fedorko P, Omastová M (2015) Study of polypyrrole aging by XPS, FTIR and conductivity measurements. *Polym Degrad Stab* 120:392–401. <https://doi.org/10.1016/j.polymdegradstab.2015.07.021>
- Sapurina I, Li Y, Alekseeva E, Bober P, Trchová M, Morávková Z, Stejskal J (2017) Polypyrrole nanotubes: the tuning of morphology and conductivity. *Polymer* 113:247–258. <https://doi.org/10.1016/j.polymer.2017.02.064>
- Kang G, Borgens RB, Cho Y (2011) Well-ordered porous conductive polypyrrole as a new platform for neural interfaces. *Langmuir* 27:6179–6184. <https://doi.org/10.1021/la104194m>
- Tan Y, Ghandi K (2013) Kinetics and mechanism of pyrrole chemical polymerization. *Synth Met* 175:183–191. <https://doi.org/10.1016/j.synthmet.2013.05.014>
- Diaz AF, Kanazawa KK, Gardini GP (1979) Electrochemical polymerization of pyrrole. *J Chem Soc Chem Commun* 635. <https://doi.org/10.1039/c39790000635>
- Bhadani SN, Kumari M, Sen Gupta SK, Sahu GC (1997) Preparation of conducting fibers via the electrochemical polymerization of pyrrole. *J Appl Polym Sci* 64:1073–1077. [https://doi.org/10.1002/\(SICI\)1097-4628\(19970509\)64:6%3c1073::AID-APP6%3e3.0.CO;2-I](https://doi.org/10.1002/(SICI)1097-4628(19970509)64:6%3c1073::AID-APP6%3e3.0.CO;2-I)
- Andriukonis E, Ramanaviciene A, Ramanavicius A (2018) Synthesis of polypyrrole induced by  $[\text{Fe}(\text{CN})_6]^{3-}$  and redox cycling of  $[\text{Fe}(\text{CN})_6]^{4-}/[\text{Fe}(\text{CN})_6]^{3-}$ . *Polymers* 10:749. <https://doi.org/10.3390/polym10070749>
- Ramanavicius A, Andriukonis E, Stirke A, Mikoliunaite L, Balevicius Z, Ramanaviciene A (2016) Synthesis of polypyrrole within the cell wall of yeast by redox-cycling of  $[\text{Fe}(\text{CN})_6]^{3-}/[\text{Fe}(\text{CN})_6]^{4-}$ . *Enzyme Microb Technol* 83:40–47. <https://doi.org/10.1016/j.enzmictec.2015.11.009>
- Andriukonis E, Stirke A, Garbaras A, Mikoliunaite L, Ramanaviciene A, Remikis V, Thornton B, Ramanavicius A (2018) Yeast-assisted synthesis of polypyrrole: quantification and influence on the mechanical properties of the cell wall. *Colloids Surf B Biointerfaces* 164:224–231. <https://doi.org/10.1016/j.colsurfb.2018.01.034>
- Shinde SS, Gund GS, Dubal DP, Jambure SB, Lokhande CD (2014) Morphological modulation of polypyrrole thin films through oxidizing agents and their concurrent effect on supercapacitor performance. *Electrochim Acta* 119:1–10. <https://doi.org/10.1016/j.electacta.2013.10.174>
- Goel S, Mazumdar NA, Gupta A (2010) Synthesis and characterization of polypyrrole nanofibers with different dopants. *Polym Adv Technol* 21:205–210. <https://doi.org/10.1016/j.electacta.2013.10.174>
- Omastová M, Trchová M, Kovářová J, Stejskal J (2003) Synthesis and structural study of polypyrroles prepared in the presence of surfactants. *Synth Met* 138:447–455. [https://doi.org/10.1016/S0379-6779\(02\)00498-8](https://doi.org/10.1016/S0379-6779(02)00498-8)
- Jiles DC (2003) Recent advances and future directions in magnetic materials. *Acta Mater* 51:5907–5939. <https://doi.org/10.1016/j.actamat.2003.08.011>
- Kahn O (2000) Chemistry and physics of supramolecular magnetic materials. *Acc Chem Res* 33:647–657. <https://doi.org/10.1021/ar9703138>
- Li XS, Zhu GT, Luo YB, Yuan BF, Feng YQ (2013) Synthesis and applications of functionalized magnetic materials in sample preparation. *TrAC Trends Anal Chem* 45:233–247. <https://doi.org/10.1016/j.trac.2012.10.015>
- Sarma DD (2001) A new class of magnetic materials:  $\text{Sr}_2\text{FeMoO}_6$  and related compounds. *Curr Opin Solid State Mater Sci* 5:261–268. [https://doi.org/10.1016/S1359-0286\(01\)00014-6](https://doi.org/10.1016/S1359-0286(01)00014-6)
- Cabrera L, Gutierrez S, Menendez N, Morales MP, Herrasti P (2008) Magnetite nanoparticles: electrochemical synthesis and characterization. *Electrochim Acta* 53:3436–3441. <https://doi.org/10.1016/j.electacta.2007.12.006>
- Stephen ZR, Kievit FM, Zhang M (2011) Magnetite nanoparticles for medical MR imaging. *Mater Today* 14:330–338. [https://doi.org/10.1016/S1369-7021\(11\)70163-8](https://doi.org/10.1016/S1369-7021(11)70163-8)
- Revia RA, Zhang M (2016) Magnetite nanoparticles for cancer diagnosis, treatment, and treatment monitoring: recent advances. *Mater Today* 19:157–168. <https://doi.org/10.1016/j.mattod.2015.08.022>
- Park DE, Chae HS, Choi HJ, Maity A (2015) Magnetite–polypyrrole Core-shell structured microspheres and their dual stimuli-response under electric and magnetic fields. *J Mater Chem C* 3:3150–3158. <https://doi.org/10.1039/C5TC00007F>
- Zhao J, Zhang S, Liu W, Du Z, Fang H (2014)  $\text{Fe}_3\text{O}_4/\text{PPy}$  composite nanospheres as anode for lithium-ion batteries with superior cycling performance. *Electrochim Acta* 121:428–433. <https://doi.org/10.1016/j.electacta.2013.12.105>
- Deng J, He C, Peng Y, Wang J, Long X, Li P, Chan ASC (2003) Magnetic and conductive  $\text{Fe}_3\text{O}_4$ -polyaniline nanoparticles with

- Core-shell structure. *Synth Met* 139:295–301. [https://doi.org/10.1016/S0379-6779\(03\)00166-8](https://doi.org/10.1016/S0379-6779(03)00166-8)
27. Singh K, Ohlan A, Kotnala RK, Bakhshi AK, Dhawan SK (2008) Dielectric and magnetic properties of conducting ferromagnetic composite of polyaniline with  $\gamma$ -Fe<sub>2</sub>O<sub>3</sub> nanoparticles. *Mater Chem Phys* 112:651–658. <https://doi.org/10.1016/j.matchemphys.2008.06.026>
  28. Kim YS, Lee SM, Govindaiah P, Lee SJ, Lee SH, Kim JH, Cheong IW (2013) Multifunctional Fe<sub>3</sub>O<sub>4</sub> nanoparticles-embedded poly(styrene)/poly(thiophene) core/shell composite particles. *Synth Met* 175:56–61. <https://doi.org/10.1016/j.synthmet.2013.04.019>
  29. Yu S-H, Yoshimura M (2002) Ferrite/metal composites fabricated by soft solution processing. *Adv Funct Mater* 12:9–15. [https://doi.org/10.1002/1616-3028\(20020101\)12:1%3c9::AID-ADFM9%3e3.0.CO;2-A](https://doi.org/10.1002/1616-3028(20020101)12:1%3c9::AID-ADFM9%3e3.0.CO;2-A)
  30. Xing Y, Jin YY, Si JC, Peng ML, Wang XF, Chen C, Cui YL (2015) Controllable synthesis and characterization of Fe<sub>3</sub>O<sub>4</sub>/Au composite nanoparticles. *J Magn Magn Mater* 380:150–156. <https://doi.org/10.1016/j.jmmm.2014.09.060>
  31. Tan L, Zhang X, Liu Q, Jing X, Liu J, Song D, Hu S, Liu L, Wang J (2015) Synthesis of Fe<sub>3</sub>O<sub>4</sub>@TiO<sub>2</sub> Core-shell magnetic composites for highly efficient sorption of uranium (VI). *Colloids Surf Physicochem Eng Asp* 469:279–286. <https://doi.org/10.1016/j.colsurfa.2015.01.040>
  32. Massart R, Cabuil V (1987) Synthèse en milieu alcalin de magnétite colloïdale: contrôle du rendement et de la taille des particules. *J Chim Phys* 84:967–973. <https://doi.org/10.1051/jcp/1987840967>
  33. Mascolo MC, Pei Y, Ring TA (2013) Room temperature coprecipitation synthesis of magnetite nanoparticles in a large pH window with different bases. *Materials* 6:5549–5567. <https://doi.org/10.3390/ma6125549>
  34. Liz L, López Quintela MA, Mira J, Rivas J (1994) Preparation of colloidal Fe<sub>3</sub>O<sub>4</sub> ultrafine particles in microemulsions. *J Mater Sci* 29:3797–3801. <https://doi.org/10.1007/BF00357351>
  35. Deng J, Peng Y, He C, Long X, Li P, Chan ASC (2003) Magnetic and conducting Fe<sub>3</sub>O<sub>4</sub>-polypyrrole nanoparticles with core-shell structure. *Polym Int* 52:1182–1187. <https://doi.org/10.1002/pi.1237>
  36. Zhao B, Nan Z (2011) Preparation of stable magnetic nanofluids containing Fe<sub>3</sub>O<sub>4</sub>@PPy nanoparticles by a novel one-pot route. *Nanoscale Res Lett* 6:230. <https://doi.org/10.1186/1556-276X-6-230>
  37. Qiao M, Lei X, Ma Y, Tian L, Su K, Zhang Q (2016) Well-Defined Core-Shell Fe<sub>3</sub>O<sub>4</sub>@polypyrrole composite microspheres with tunable shell thickness: synthesis and their superior microwave absorption performance in the Ku band. *Ind Eng Chem Res* 55:6263–6275. <https://doi.org/10.1021/acs.iecr.5b04814>
  38. Zhang WD, Xiao HM, Zhu LP, Fu SY, Wan MX (2010) Facile one-step synthesis of electromagnetic functionalized polypyrrole/Fe<sub>3</sub>O<sub>4</sub> nanotubes via a self-assembly process. *J Polym Sci Part Polym Chem* 48:320–326. <https://doi.org/10.1002/pola.23787>
  39. Kalska-Szostko B, Rogowska M, Dubis A, Szymański K (2012) Enzymes immobilization on Fe<sub>3</sub>O<sub>4</sub>-gold nanoparticles. *Appl Surf Sci* 258:2783–2787. <https://doi.org/10.1016/j.apsusc.2011.10.132>
  40. Pang SC, Chin SF, Anderson MA (2007) Redox equilibria of iron oxides in aqueous-based magnetite dispersions: effect of pH and redox potential. *J Colloid Interface Sci* 311:94–101. <https://doi.org/10.1016/j.jcis.2007.02.058>
  41. Andrieux CP, Audebert P, Hapiot P, Saveant JM (1990) Observation of the cation radicals of pyrrole and of some substituted pyrroles in fast-scan cyclic voltammetry. Standard potentials and lifetimes. *J Am Chem Soc* 112:2439–2440. <https://doi.org/10.1021/ja00162a065>
  42. Chen S, Liu H, Wang Y, Xu YS, Liu W, He D, Liu X, Liu J, Hu C (2017) Electrochemical capacitance of spherical nanoparticles formed by electrodeposition of intrinsic polypyrrole onto Au electrode. *Electrochim Acta* 232:72–79. <https://doi.org/10.1016/j.electacta.2017.02.133>
  43. Scharifker BR, Fermin DJ (1994) The role of intermediates in solution in the initial stages of electrodeposition of polypyrrole. *J Electroanal Chem* 365:35–39. [https://doi.org/10.1016/0022-0728\(93\)02993-R](https://doi.org/10.1016/0022-0728(93)02993-R)
  44. Zheng W, Razal JM, Spinks GM, Truong VT, Whitten PG, Wallace GG (2012) The role of unbound oligomers in the nucleation and growth of electrodeposited polypyrrole and method for preparing high strength, high conductivity films. *Langmuir* 28:10891–10897. <https://doi.org/10.1021/la301701g>
  45. Garfias-García E, Romero-Romo M, Ramírez-Silva MT, Morales J, Palomar-Pardavé M (2010) Electrochemical nucleation of polypyrrole onto different substrates. *Int J Electrochem Sci* 5
  46. Fermin DJ, Scharifker BR (1993) Products in solution during electrodeposition of polypyrrole. *J Electroanal Chem* 357:273–287. [https://doi.org/10.1016/0022-0728\(93\)80385-U](https://doi.org/10.1016/0022-0728(93)80385-U)
  47. Guyard L, Hapiot P, Neta P (1997) Redox chemistry of bipyroles: further insights into the oxidative polymerization mechanism of pyrrole and oligopyrroles. *J Phys Chem B* 101:5698–5706. <https://doi.org/10.1021/jp9706083>
  48. Saraç AS, Sönmez G (2002) Spectroelectrochemistry of pyrrole oligomers in the presence of acrylamide. *Polym Int* 51:594–600. <https://doi.org/10.1002/pi.914>
  49. Stolarz A, Szydłowski J (1994) Kinetics of tritium isotope exchange between liquid pyrrole and gaseous hydrogen. *J Radioanal Nucl Chem* 185:219–226. <https://doi.org/10.1007/BF02041294>
  50. Schwartz CP, Uejio JS, Duffin AM, England AH, Prendergast D, Saykally RJ (2009) Auto-oligomerization and hydration of pyrrole revealed by x-ray absorption spectroscopy. *J Chem Phys* 131:114509. <https://doi.org/10.1063/1.3223539>
  51. Hawkins SJ, Ratcliffe NM (2000) A study of the effects of acid on the polymerisation of pyrrole, on the oxidative polymerisation of pyrrole and on polypyrrole. *J Mater Chem* 10:2057–2062. <https://doi.org/10.1039/B001912G>
  52. Wysocka-Zolopa M, Goclon J, Basa A, Winkler K (2018) Polypyrrole nanoparticles doped with fullerene uniformly distributed in the polymeric phase: synthesis, morphology, and electrochemical properties. *J Phys Chem C* 122:25539–25554. <https://doi.org/10.1021/acs.jpcc.8b07681>
  53. Goclon J, Winkler K (2018) Band gap tuning in composites of polypyrrole derivatives and C<sub>60</sub>Pd<sub>3</sub> polymer as models for p–n junction: a first principle computational study. *ChemistrySelect* 3:373–383. <https://doi.org/10.1002/slct.201702752>
  54. Wang Y, Zou B, Gao T, Wu X, Lou S, Zhou S (2012) Synthesis of orange-like Fe<sub>3</sub>O<sub>4</sub>/PPy composite microspheres and their excellent Cr(VI) ion removal properties. *J Mater Chem* 22:9034–9040. <https://doi.org/10.1039/C2JM30440F>
  55. Peng X, Zhang W, Gai L, Jiang H, Wang Y, Zhao L (2015) Dedoped Fe<sub>3</sub>O<sub>4</sub>/PPy nanocomposite with high anti-interfering ability for effective separation of Ag(I) from mixed metal-ion solution. *Chem Eng J* 280:197–205. <https://doi.org/10.1016/j.cej.2015.05.118>
  56. Biesinger MC, Payne BP, Grosvenor AP, Lau LWM, Gerson AR, Smart RSC (2011) Resolving surface chemical states in XPS analysis of first row transition metals, oxides and hydroxides: Cr, Mn, Fe, Co and Ni. *Appl Surf Sci* 257:2717–2730. <https://doi.org/10.1016/j.apsusc.2010.10.051>
  57. Wilson D, Langell MA (2014) XPS analysis of oleylamine/oleic acid capped Fe<sub>3</sub>O<sub>4</sub> nanoparticles as a function of temperature. *Appl Surf Sci* 303:6–13. <https://doi.org/10.1016/j.apsusc.2014.02.006>
  58. Cheng FY, Su CH, Yang YS, Yeh CS, Tsai CY, Wu CL, WuMT SDB (2005) Characterization of aqueous dispersions of Fe<sub>3</sub>O<sub>4</sub> nanoparticles and their biomedical applications. *Biomaterials* 26:729–738. <https://doi.org/10.1016/j.biomaterials.2004.03.016>

59. Kolen'ko YV, Bañobre-López M, Rodríguez-Abreu C, Carbó-Argibay E, Sailsman A, Piñeiro-Redondo Y, Cerqueira MF, Petrovykh DY, Kovnir K, Lebedev OI, Rivas J (2014) Large-scale synthesis of colloidal Fe<sub>3</sub>O<sub>4</sub> nanoparticles exhibiting high heating efficiency in magnetic hyperthermia. *J Phys Chem C* 118:8691–8701. <https://doi.org/10.1021/jp500816u>
60. Rajagopalan R, Iroh JO (2003) Characterization of polyaniline–polypyrrole composite coatings on low carbon steel: a XPS and infrared spectroscopy study. *Appl Surf Sci* 218:58–69. [https://doi.org/10.1016/S0169-4332\(03\)00579-8](https://doi.org/10.1016/S0169-4332(03)00579-8)
61. Wuang SC, Neoh KG, Kang E-T, Pack DW, Leckband DE (2007) Synthesis and functionalization of polypyrrole-Fe<sub>3</sub>O<sub>4</sub> nanoparticles for applications in biomedicine. *J Mater Chem* 17:3354–3362. <https://doi.org/10.1039/B702983G>
62. Malitesta C, Losito I, Sabbatini L, Zambonin PG (1995) New findings on polypyrrole chemical structure by XPS coupled to chemical derivatization labelling. *J Electron Spectrosc Relat Phenom* 76:629–634. [https://doi.org/10.1016/0368-2048\(95\)02438-7](https://doi.org/10.1016/0368-2048(95)02438-7)
63. Qiu G, Wang Q, Nie M (2006) Polypyrrole-Fe<sub>3</sub>O<sub>4</sub> magnetic nanocomposite prepared by ultrasonic irradiation. *Macromol Mater Eng* 291:68–74. <https://doi.org/10.1002/mame.200500285>
64. Janem N, Azizi ZS, Tehrani MM (2021) Microwave absorption and magnetic properties of thin-film Fe<sub>3</sub>O<sub>4</sub> @polypyrrole nanocomposites: the synthesis method effect. *Synth Met* 282:116948. <https://doi.org/10.1016/j.synthmet.2021.116948>
65. Mo Z, Gou H, He J, Wang JJ, Guo R (2014) Preparation and characterization of conductive and magnetic PPy/Fe<sub>3</sub>O<sub>4</sub>/Ag nanocomposites. *Polym Compos* 35:450–455. <https://doi.org/10.1002/pc.22680>
66. Jureviciute I, Bruckenstein S (2003) Electrochemical activity of chemically deposited polypyrrole films. *J Solid State Electrochem* 7:554–560. <https://doi.org/10.1007/s10008-003-0384-x>
67. Sahoo S, Karthikeyan G, Nayak GCh, Das CK (2011) Electrochemical characterization of in situ polypyrrole coated graphene nanocomposites. *Synth Met* 161:1713–1719. <https://doi.org/10.1016/j.synthmet.2011.06.011>
68. Kim J-H, Sharma AK, Lee Y-S (2006) Synthesis of polypyrrole and carbon nano-fiber composite for the electrode of electrochemical capacitors. *Mater Lett* 60:1697–1701. <https://doi.org/10.1016/j.matlet.2005.12.002>
69. Bard AJ, Faulkner LR (1980) *Electrochemical methods*, 2nd ed. Wiley, New York p. 522
70. Kuwabata S, Yoneyama H, Tamura H (1984) Redox behavior and electrochromic properties of polypyrrole films in aqueous solutions. *Bull Chem Soc Jpn* 57:2247–2253. <https://doi.org/10.1246/bcsj.57.2247>
71. Akhtar AJ, Mishra S, Saha SK (2020) Charge transport mechanism in reduced graphene oxide/polypyrrole based ultrahigh energy density supercapacitor. *J Mater Sci Mater Electron* 31:11637–11645. <https://doi.org/10.1007/s10854-020-03714-y>
72. Huang Y, Li H, Wang Z, Zhu M, Pei Z, Xue Q, Huang Y, Zhi C (2016) Nanostructured polypyrrole as a flexible electrode material of supercapacitor. *Nano Energy* 22:422–438. <https://doi.org/10.1016/j.nanoen.2016.02.047>
73. Ramesh S, Yadav HM, Karuppasamy K, Vikraman D, Hs K, Kim JH, Kim HS (2019) Fabrication of manganese oxide@nitrogen doped graphene oxide/polypyrrole (MnO<sub>2</sub>@NGO/PPy) hybrid composite electrodes for energy storage devices. *J Mater Res Technol* 8:4227–4238. <https://doi.org/10.1016/j.jmrt.2019.07.033>
74. Samukaite-Bubniene U, Valiūnienė A, Bucinskas V, Genys P, Ratautaitė V, Ramanaviciene A, Aksun E, Tereshchenko A, Zeybek B, Ramanavicius A (2021) Towards supercapacitors: cyclic voltammetry and fast Fourier transform electrochemical impedance spectroscopy based evaluation of polypyrrole electrochemically deposited on the pencil graphite electrode. *Colloids Surf Physicochem Eng Asp* 610:125750. <https://doi.org/10.1016/j.colsurfa.2020.125750>

**Publisher's Note** Springer Nature remains neutral with regard to jurisdictional claims in published maps and institutional affiliations.